

Polyelectrolyte adsorption on an oppositely charged spherical polyelectrolyte brush

Cite this: *Soft Matter*, 2013, **9**, 5087

Qianqian Cao* and Michael Bachmann*

Coarse-grained molecular dynamics simulations are performed to investigate the interaction and complex formation of a spherical polyelectrolyte brush (SPB) consisting of uniformly distributed grafted polyelectrolytes (GPE) and an oppositely charged linear polyelectrolyte (LPE). This system is considered as a model for complexation of a polyelectrolyte and a soft nanoparticle. The effects of the LPE rigidity, length of the GPE chains, grafting density and core radius on complexation behavior are addressed. Depending on these parameters the GPE layer exhibits different structures, and acts on the LPE like a bare charged sphere, brush or star-like polyelectrolyte. Unlike the charged-sphere case, where the LPE binds to the solid body of the nanoparticle, the GPE arms can bind partly or completely to the LPE which in these cases is less affected by the core surface. The rigidity of the LPE also influences the conformational behavior of the brush layer. If the grafting density is small, the semiflexible LPE adopts a highly ordering solenoid conformation on the surface of the highly charged sphere. The ordered arrangement is disrupted as the GPE length increases. A higher ordering degree is also found for the semiflexible LPE at an intermediate core radius and relatively low grafting density. If the amount of surface charges is fixed, short GPEs suppress the complexation of the LPE with the SPB, compared to the cases of the long GPEs and bare charged sphere. However, the complexation propensity increases for lower grafting densities. Its dependence on the core radius is significantly different for flexible and semiflexible LPEs.

Received 15th March 2013

Accepted 3rd April 2013

DOI: 10.1039/c3sm50754h

www.rsc.org/softmatter

1 Introduction

Understanding the fundamental adsorption process and conformational transition of polyelectrolytes at charged surfaces is of great importance for a wide spectrum of biological and nanotechnological applications.^{1,2} Polyelectrolytes are polymer chains which consist of repeating monomer units having electrolyte groups and exist ubiquitously in nature. Prominent examples are DNA and RNA in biological systems. It is well known that each nucleosome (the lowest-level complex structure for chromatin) consists of 146 base pairs of DNA wrapped around a histone octamer in 1.67 turns of a left-handed superhelix. Revealing the underlying formation mechanism of the nucleosome is crucial to understand the hierarchical structure and dynamics of chromatin.³ Furthermore, the complexation of DNA with oppositely charged objects *in vitro* seems to be a promising model system to investigate fundamental mechanisms of the natural packing of DNA by histone octamers. Examples include DNA compaction by nanoparticles,^{4,5} proteins⁶ and dendrimers.⁷ The charge inversion or overcharging usually occurs in the complexation process of polyelectrolytes with oppositely charged nanoparticles. Theoretically, the overcharging of histone octamers or

nanoparticles wrapped by DNA is assumed to be caused by repulsion of non-compensated charges on the outer DNA surface.⁸

A large number of computational and analytical works on the complexation of linear polyelectrolytes (LPE) with oppositely charged nanoparticles have been performed.^{9–17} These works have addressed various properties of the polyelectrolyte–nanoparticle complexes and effects of different parameters (including temperature, salt concentration, surface charge density and size of the particle, chain length, linear charge density, and stiffness of the polyelectrolyte) on the conformational behavior of adsorbed polyelectrolytes. It was found that the degree of overcharging rises with a decrease in the intrinsic rigidity of the polyelectrolyte and an increase in the diameter of the particle.^{12,14} For flexible polyelectrolyte chains, the increase of salt concentration favors charge inversion.¹¹ Additionally, an important problem of polyelectrolyte–particle complexation is how to control the chain conformation by tuning the solution properties and structural parameters of charged particles. Histone proteins can compact a centimeter long DNA chain into a cellular nucleus with the size of a few micrometers. Related experimental and theoretical studies indicate that DNA exhibits a highly ordered structure when it is in a condensed state under proper physiological conditions. The ordered conformation of DNA chain suffers serious damage (that is, the chain wraps disorderly around the particle) when the chain becomes more

Center for Simulational Physics, The University of Georgia, Athens, Georgia 30602, USA. E-mail: qqcao@uga.edu; bachmann@smsyslab.org

flexible. This effect can be simulated by elevating the salt concentration.¹⁸ The investigations on simpler model systems (referring to the interaction of polyelectrolytes with oppositely charged spherical particles) reveal that by increasing the intrinsic rigidity, the polyelectrolyte undergoes a transition from a disordered conformation to an ordered solenoid conformation.¹³ The adsorption amount and equilibrium structure of the polyelectrolyte on the particle surface depend on the competition among the chain intrinsic stiffness, electrostatic repulsion between charged monomers and electrostatic attractive interaction between the monomers and the particle.^{13,14,16,17} The adsorption reaches a balance under the influences of forcing the chain to straighten (chain rigidity and electrostatic repulsion) and inducing its collapse (electrostatic attraction). The surface curvature of the particle limits the amount of adsorbed monomers of the polyelectrolyte:⁹ the overcharging of the particle is enhanced with the increase of its diameter up to a complete collapse of the chain.

In addition to the complexation of polyelectrolytes with spherical objects, the interaction and aggregate formation of polyelectrolytes with other oppositely charged objects, such as cylinders,^{10,19} surfactants,^{20,21} dendrimers,^{7,22} and micelles²³ have been investigated experimentally and theoretically. Polyelectrolytes adsorbed onto oppositely charged bare and impenetrable surfaces may be regarded as well-understood systems. However, insufficient attention has been paid to understand the complexation of polyelectrolytes with penetrable objects (such as branched polymers) at molecular level. For example, dendrimers can be used as nanocontainers to control the drug delivery and release processes. If the “guest” molecules are LPE chains, typically DNA, the formed complex might be interesting for potential biomedical applications. The penetrable objects do not possess a clearly defined surface and allow polyelectrolytes to penetrate inside, which leads to a more complicated local structure. Moreover, the phase transition and structural properties of the complex accompanying the overcharging of penetrable objects by polyelectrolytes have not been clearly addressed yet. Regarding structural phases, several recent studies have revealed a complex hierarchy of conformational transition, in nucleation processes of flexible^{24–27} and semiflexible polymers,²⁸ as well as aggregates.^{29,30} The thermodynamics of polymer adsorption process at soft³¹ and solid substances^{32–35} has also been investigated thoroughly.

The investigation of polyelectrolyte brushes is quite challenging, but their importance for biology and material science is striking.^{36–38} The long-range electrostatic interaction within them brings about a variety of novel properties compared to polymer layers consisting of end-grafted neutral macromolecules. Moreover, they can respond to various external and internal stimuli, such as salt concentration, grafting density, pH, temperature, electric field, and charge fraction of the chain. Experimentally, chemists have designed and synthesized a number of novel polyelectrolyte brush systems with various specific functions that possess potential for controlling colloid stability,³⁹ flow regulation,⁴⁰ and for applications such as smart sensors.⁴¹ In addition, a large number of studies of the theory for polyelectrolyte brushes were performed to understand their

conformational characteristics, interactions, and phase behavior using scaling predictions^{42–44} and self-consistent-field calculations.^{45–47} Several publications have reported the interaction of SPBs with oppositely charged linear polymers such as surfactants^{48,49} and short polyelectrolyte chains.⁵⁰ However, much less is known about how to drive the complexation of an SPB and a single long LPE. The purpose of this work is to study the complex formation between a long polyelectrolyte chain and a spherical polyelectrolyte brush (SPB) using coarse-grained molecular dynamics simulations. The SPB consists of a spherical, solid core and penetrable surface layer of GPEs. For low grafting density or short GPEs, it resembles a hard nanoparticle. If the grafting density is sufficiently high and the GPEs are long enough, the SPB mimics a soft nanoparticle. Here, we systematically investigate how the binding properties of the LPE depend on grafting density, core radius, and LPE stiffness.

The remainder of the paper is organized as follows. In the next section, the model system and simulation method are described. Following that, we present our simulation results and discuss the conformational transition and complexation properties of the LPE-SPB complex under influences of core size, GPE length, LPE rigidity, and grafting number in Section 3. Finally, our conclusions are summarized in Section 4.

2 Model and simulation method

Molecular dynamics (MD) simulations are used to study the conformational behavior of the complex of a spherical polyelectrolyte brush (SPB) with a long linear polyelectrolyte (LPE) based on a coarse-grained bead-spring model. The SPB considered in this work consists of a spherical core uniformly grafted with N_g fully flexible polyelectrolyte chains. A GPE chain contains N_{gm} monomers, each of which carries a positive charge $+e$. The grafting density of the SPB is $\rho_g = N_g/4\pi R^2$, where R is the radius of the core. For fixed core radius, we will also use the grafting number N_g to characterize the density of GPE chains. The LPE includes $N_{lm} = 200$ monomers, each with a negative charge $-e$. To neutralize the system, monovalent ions are added; $N_{gm}N_g$ anions and N_{lm} cations are dissociated from the GPEs and LPE, respectively. All particles are enclosed in a cubic simulation box with edge lengths $L = 250\sigma$. The particle diameter σ is chosen to be the same for all particle types. Periodic boundary conditions are applied in all three directions. Our simulation box is large enough to avoid short-range interactions of the LPE with its periodic images.

The short-range interaction between any two nonbonded particles separated by a distance r is modeled by the truncated-shifted Lennard-Jones (LJ) potential

$$U_{LJ}(r) = \begin{cases} 4\epsilon_{LJ} \left[(\sigma/r)^{12} - (\sigma/r)^6 - (\sigma/r_c)^{12} + (\sigma/r_c)^6 \right], & r < r_c \\ 0, & r \geq r_c \end{cases} \quad (1)$$

where ϵ_{LJ} is the interaction strength, σ is the particle diameter chosen to be the same irrespective of the particle type, and r_c is the cutoff distance beyond which the LJ interaction is ignored. The cutoff distance is set to be $r_c = 2^{1/6}\sigma$, corresponding to a

purely repulsive interaction between the particles. In this paper, σ , m , and ε_{LJ} define the length, mass, and energy units, respectively. All other units are derived from these basic units, such as time unit $\tau = (m\sigma^2/\varepsilon_{\text{LJ}})^{1/2}$ and temperature unit $T^* = \varepsilon_{\text{LJ}}/k_{\text{B}}$ (k_{B} is the Boltzmann constant). The GPE and LPE chains are modeled using a widely utilized, coarse-grained bead-spring model. Bonded interaction between beads is modeled by the finitely extendable nonlinear elastic (FENE) potential⁵¹

$$U_{\text{bond}}(r_{ii+1}) = \begin{cases} -(k_i R_0^2/2) \ln(1 - r_{ii+1}^2/R_0^2), & r_{ii+1} < R_0 \\ \infty, & r_{ii+1} \geq R_0 \end{cases} \quad (2)$$

where r_{ii+1} is the distance between bonded beads. The maximum bond length is $R_0 = 1.5\sigma$ and the spring constant is given by $k_i = 30\varepsilon_{\text{LJ}}/\sigma^2$. The combination of LJ and FENE potentials ensures that the constituent chains cannot cross through one another. One end monomer of each chain from the SPB is anchored onto the core surface. All particles except the grafted monomers interact repulsively with the core through a LJ potential with a shifted distance of the core radius R

$$U_{\text{wall}}(r) = U_{\text{LJ}}(r - R). \quad (3)$$

The bending rigidity of the LPE chain is modeled by using the harmonic angle potential

$$U_{\text{angle}}(\theta) = k_{\theta}(\theta - \theta_0)^2, \quad (4)$$

where θ is the bond angle and k_{θ} is the bond stiffness. The equilibrium value of the bond angle θ_0 is set to 180° . A fully flexible chain is mimicked by setting $k_{\theta} = 0$, and $k_{\theta} = 300k_{\theta}^*$ corresponds to a strong chain stiffness, where $k_{\theta}^* = \varepsilon_{\text{LJ}}/\text{rad}^2$ is the chain stiffness unit.

Electrostatic interaction between any two charged particles, separated by a distance r_{ij} and with charge valences Z_i and Z_j , is described by the Coulomb potential

$$U_{\text{coul}}(r_{ij}) = k_{\text{B}} T Z_i Z_j \frac{\lambda_{\text{B}}}{r_{ij}}, \quad (5)$$

where the Bjerrum length $\lambda_{\text{B}} = e^2/(4\pi\varepsilon_0\varepsilon_r k_{\text{B}} T)$ is the distance at which the electrostatic energy between two elementary charges is comparable in magnitude to the thermal energy $k_{\text{B}} T$. We choose $\sigma = \lambda_{\text{B}}$ for all simulations. The system resides in implicit aqueous solvent. Therefore, we choose $\lambda_{\text{B}} = 0.71$ nm and $\varepsilon_r = 80.4$ for water at room temperature (293 K). The sum of long-range electrostatic interactions is calculated using the particle-particle/particle-mesh (PPPM) algorithm, which maps charges to a 3D mesh and uses fast Fourier transforms (FFTs) to solve Poisson's equation on the mesh.⁵²

The system temperature is controlled by a Langevin thermostat, which is based on the fluctuation-dissipation theorem.⁵³ In this approach, the motion of each particle is determined by the following equation

$$m \frac{d\mathbf{v}_i(t)}{dt} = \mathbf{F}_i - \gamma m \mathbf{v}_i(t) + \mathbf{F}_i^{\text{f}}(t), \quad (6)$$

where \mathbf{F}_i is the deterministic force acting on particle i from other particles. All particles have the same mass. The friction coefficient γ is used to control the relaxation rate of the temperature

and is related to the viscosity of the solvent. \mathbf{F}_i^{f} is a stochastic force which is sampled from the Gaussian distribution

$$\langle \mathbf{F}_i^{\text{f}}(t) \rangle = 0, \quad \langle \mathbf{F}_i^{\text{f}}(t) \cdot \mathbf{F}_j^{\text{f}}(t') \rangle = 6m\gamma k_{\text{B}} T \delta_{ij} \delta(t - t'), \quad (7)$$

where $\langle \dots \rangle$ denotes the ensemble average of the function enclosed and T is the desired temperature. γ and T are set to $1.0\tau^{-1}$ and $1.0T^*$, respectively. The stationary solution of the Langevin equation corresponds to a Boltzmann distribution, and thus the simulation is performed in the canonical NVT ensemble. The positions and velocities of the particles are calculated using the velocity-Verlet algorithm.^{54,55} All simulations are conducted with a time step $\Delta t = 0.008\tau$. Initially, the counterions are randomly dispersed within the simulation region. The GPE chains stretch normal to the grafting surface. The LPE has an initial extended conformation and keeps a distance of $N_{\text{gm}}\sigma + R$ from the center of the SPB. An equilibrium run of 1×10^6 time steps is first performed, then followed by a production run of 2×10^6 time steps to obtain the equilibrium properties of the system. Molecular dynamics simulations were carried out using the open-source, massively parallel software LAMMPS.⁵⁶

3 Results and discussion

3.1 Effect of the grafting density

In this section, we study how the grafting density influences the complexation of the LPE with the SPB. Fig. 1 gives the chain radius of gyration as a function of the grafting number N_{g} . The core radius and GPE length are fixed at $R = 7\sigma$ and $N_{\text{gm}} = 20$, respectively. The mean radius of gyration $\langle R_{\text{lg}} \rangle$ of the LPE shows a maximum at the smallest N_{g} studied, $N_{\text{g}} = 6$ ($\rho_{\text{g}} = 0.0097\sigma^{-2}$). With increasing N_{g} , $\langle R_{\text{lg}} \rangle$ remains approximately constant. This corresponds to a completely collapsed state of the LPE. Compared with the flexible LPE ($k_{\theta} = 0$), the semiflexible LPE with a stiffness $k_{\theta} = 300k_{\theta}^*$ has a larger value of $\langle R_{\text{lg}} \rangle$ at all grafting numbers or densities. Note that $\langle R_{\text{lg}} \rangle$ of the flexible LPE at $N_{\text{g}} = 6$ is comparable to the size of the core and is not significantly larger than that at higher N_{g} , which represents a shrinkage conformation of the flexible LPE though for sparse grafting.

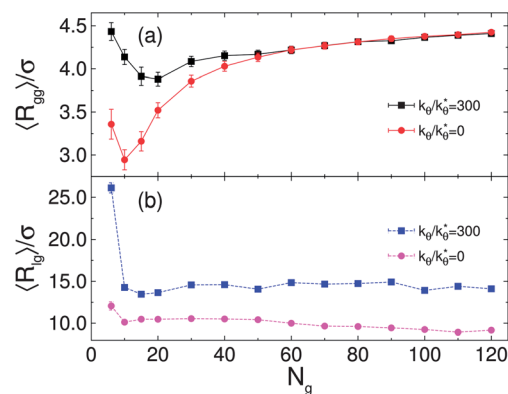


Fig. 1 Average radius of gyration of (a) the GPEs $\langle R_{\text{gg}} \rangle$ and (b) the LPE $\langle R_{\text{lg}} \rangle$ as a function of the grafting density at $k_{\theta} = 0$ and $k_{\theta} = 300k_{\theta}^*$. Simulation results were obtained with $R = 7\sigma$ and $N_{\text{gm}} = 20$.

To obtain a clear picture of the complexation, Fig. 2 shows snapshots of LPE-SPB complexes at different grafting densities for the semiflexible (Fig. 2a–d) and for the flexible LPE (Fig. 2e–h). We find that the arms of the SPB hold on to the LPE due to electrostatic attraction between them which induces bending of the semiflexible LPE. At $N_g = 6$, the semiflexible LPE chain is in a folded state but does not collapse onto the surface of the SPB (Fig. 2a). Moreover, the GPEs are also straightened strongly. As the number of arms increases, the adsorption energy becomes large enough to entirely overcome the rigidity of the LPE. The LPE chain wraps around the core and adopts a solenoid-like conformation. Unlike the case of a bare charged surface, the LPE chain is not adsorbed on the core surface. The GPE chains keep it at a significant distance from the core surface. Only an end part of grafted chains is entangled with the semiflexible LPE. At higher grafting densities, such as $N_g = 40$ ($\rho_g = 0.065\sigma^{-2}$) and 120 ($0.19\sigma^{-2}$), not all chains have a direct contact with the LPE (Fig. 2c and d). Especially at $N_g = 120$, most grafted chains adopt an extended conformation perpendicular to the grafting surface. Moreover, a considerable amount of counterions accumulates within the GPE layer, which has strong screening effects on electrostatic interactions between the LPE and the GPE chains. The flexible LPE exhibits a coil conformation and collapses on the core surface even at the smallest N_g . Additionally, no obvious conformational change is

observed for the flexible LPE chain. At $N_g = 120$, the flexible LPE is entirely embedded into the brush (Fig. 2h).

It is particularly instructive for the understanding of the complex interplay of LPE charges, GPE charges, and counterions to investigate the average radius of gyration of the GPE chains as a function of the number of grafted chains, $\langle R_{gg} \rangle(N_g)$. As it can be seen in Fig. 1a, it is minimal, where also $\langle R_{lg} \rangle(N_g)$ possesses a minimum (independently of the LPE stiffness). This means, the low grafting density allows the GPEs to optimally bind to the LPE without influencing each other too much. The GPEs effectively behave like flexible polymers. If the number of GPEs is increased, however, the mutual repulsion among the GPEs increases and they try to avoid each other; their effective stiffness increases. This behavior is partly compensated by the counterions. Their density dramatically increases near the nanoparticle. In effect, whereas $\langle R_{lg} \rangle(N_g)$ remains almost constant for larger GPE grafting densities, $\langle R_{gg} \rangle(N_g)$ consequently increases because of the effects described. The entire nanoparticle resembles a brush that accommodates the LPE completely, if N_g is large enough.

To investigate the wrapping conformation of the LPE around the core, we introduce the order parameter η by⁵⁷

$$\eta = \frac{\left| \sum_{(i)} \mathbf{r}_{i,i+1} \times \mathbf{r}_{i+1,i+2} \right|}{N_{gm}} \quad (8)$$

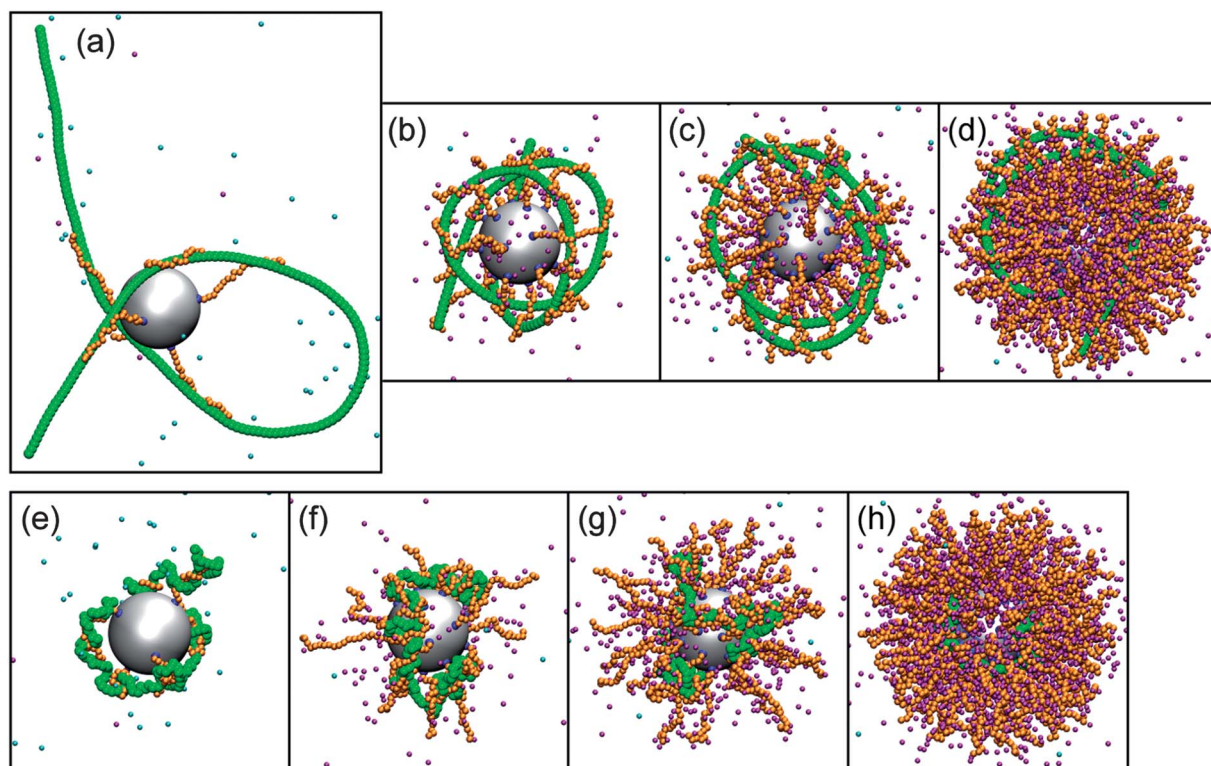


Fig. 2 Typical simulation snapshots of the LPE-SPB complexes at different grafting densities with $R = 7\sigma$ and $N_{gm} = 20$. (a)–(d) for the semiflexible LPE correspond to $N_g = 6$ ($\rho_g = 0.0097\sigma^{-2}$), 20 ($0.032\sigma^{-2}$), 40 ($0.065\sigma^{-2}$) and 120 ($0.19\sigma^{-2}$), respectively. (e)–(h) for the flexible LPE correspond to the same grafting densities as (a)–(d). The LPE and GPE chains are shown in green and orange, respectively. Blue and gray beads represent grafted monomers and spherical core, respectively. Counterions from the LPE and GPE chains are shown in cyan and purple, respectively. All images of conformations shown throughout the paper were generated by using VMD.⁶⁰

where $\mathbf{r}_{i,i+1}$ is the unit bond vector between monomers i and $i + 1$. When the LPE wraps orderly around the core, the direction of each vector product between $\mathbf{r}_{i,i+1}$ and its adjacent vector is nearly parallel to the helical axis of the LPE chain. In our previous studies, it was found that misfolded conformations are formed at $\eta < 0.05$.⁵⁸ Wrapping conformations of the flexible LPE are typically disordered, but some possess an interesting characteristic shape. For example, a corolla structure is representative in cases of long grafted chains (Fig. 8g and h), but such structures cannot suitably be characterized quantitatively by using η .

For the semiflexible LPE, the dependence of η on the number of grafted chains N_g is shown in Fig. 3. For lowest N_g , the order parameter has a very small value because of the presence of two long end segments of the LPE, which are not complexed with the GPEs. By increasing N_g , the ordering degree of the LPE around the core is largely improved, then followed by a decrease. Increasing η leads to the formation of an ordered structure with an increased number of wrapping turns that resembles a solenoid. For GPE lengths $10 \leq N_{gm} \leq 40$, all or most grafted chains are bound to the LPE, which is in a fully collapsed state (Fig. 1b). The semiflexible LPE maintains the solenoid-like conformation. However, we find that, by further increasing the number of grafted chains to larger values $N_g > 80$ ($\rho_g = 0.13\sigma^{-2}$), the conformation of the LPE has a significant dependence on its initial conformations. This means that the simulation got trapped in a local minimum of the free-energy landscape and a reasonable analysis breaks down. The reason is that at large grafting densities, the interchain separation is decreased considerably while the charge distribution in the brush layer becomes dense. Moreover, the SPB carries a much higher amount of charges than the LPE. The number of grafted chains bound to the LPE increases largely though the number of absorbed monomers from each grafted chain is reduced. The increased number of GPE chains, which complex to the LPE, causes a strong conformational restraint. Additionally, stronger repulsive interactions in the dense brush layer promote the stretching of grafted chains. Moreover, the dense arrangement of grafted chains also limits the movement of the LPE. As a consequence, when the LPE with a different initial conformation is trapped in the denser brush layer, more residues from

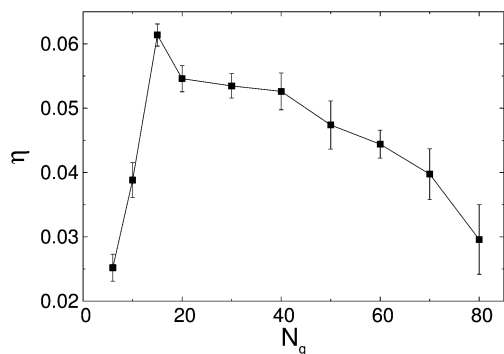


Fig. 3 Ordering parameter η of the semiflexible LPE around the core as a function of the grafting density at $R = 7\sigma$ and $N_{gm} = 20$.

the initial conformation are almost immobile due to strong electrostatic attraction and entropic constraints.

3.2 Core radius dependence

Fig. 4 shows the radius of gyration of the LPE and GPE chains $\langle R_{lg} \rangle$ and $\langle R_{gg} \rangle$, respectively, as a function of the core radius R for $N_g = 15$ grafted chains with length $N_{gm} = 20$ each. As expected, $\langle R_{lg} \rangle$ increases almost linearly with larger core radii (Fig. 4b). At the smallest radius $R = 2\sigma$, the LPE chain is condensed significantly. Conversely, the GPE chains are not most compact. In fact, $\langle R_{gg} \rangle$ has a larger value compared to the cases of larger core radius such as $R = 7\sigma$ (Fig. 4a). In particular, for semiflexible LPE $\langle R_{gg} \rangle$ reaches a maximum value at $R = 2\sigma$ in the range of the studied parameter interval. Obviously, very high bending energy due to strong shrinkage of the LPE leads to the straightening of grafted chains. At small R , the reduction of $\langle R_{gg} \rangle$ upon increasing the core radius is caused by the release of bending energy of the LPE, which corresponds to an increase of $\langle R_{lg} \rangle$. When $\langle R_{gg} \rangle$ decreases to a minimum value, a further increase of the core radius leads to a growing radius of gyration of grafted chains. Because the number of grafted chains is constant, increasing the core radius results in a larger separation between grafting points. Therefore, the probability of contacts between the LPE and GPE chains drops, especially at large core radius. The reduced degree of complexation brings about an increased average radius of gyration of grafted chains. The free GPEs (not complexed to the LPE) adopt stretched conformations due to electrostatic repulsion between charged monomers. We will discuss the degree of LPE–GPE complexation in more detail below. Furthermore, the effect of the bending energy of the LPE on $\langle R_{gg} \rangle$ becomes weak as the core radius increases. It can be verified from the decreased difference of $\langle R_{gg} \rangle$ for cases of semiflexible and flexible LPE chains. This also means that the core radius as a parameter starts to become dominant in controlling the conformational behavior of the LPE. Similarly, one can observe that the radius of gyration of the semiflexible LPE and that of the flexible LPE approach each other when the core radius becomes larger.

Snapshots of the LPE–SPB complex at different core radius are shown in Fig. 5. At the largest core radius studied, $R = 21\sigma$,

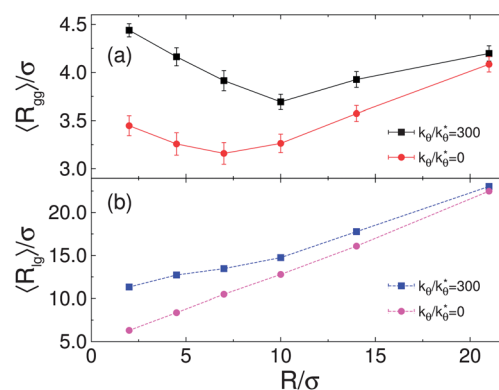


Fig. 4 Average radius of gyration of (a) the GPEs $\langle R_{gg} \rangle$ and (b) the LPE $\langle R_{lg} \rangle$ as a function of the core radius at $k_{\theta} = 0$ and $k_{\theta} = 300k_{\theta}^*$. Simulation results were obtained with $N_g = 15$ and $N_{gm} = 20$.

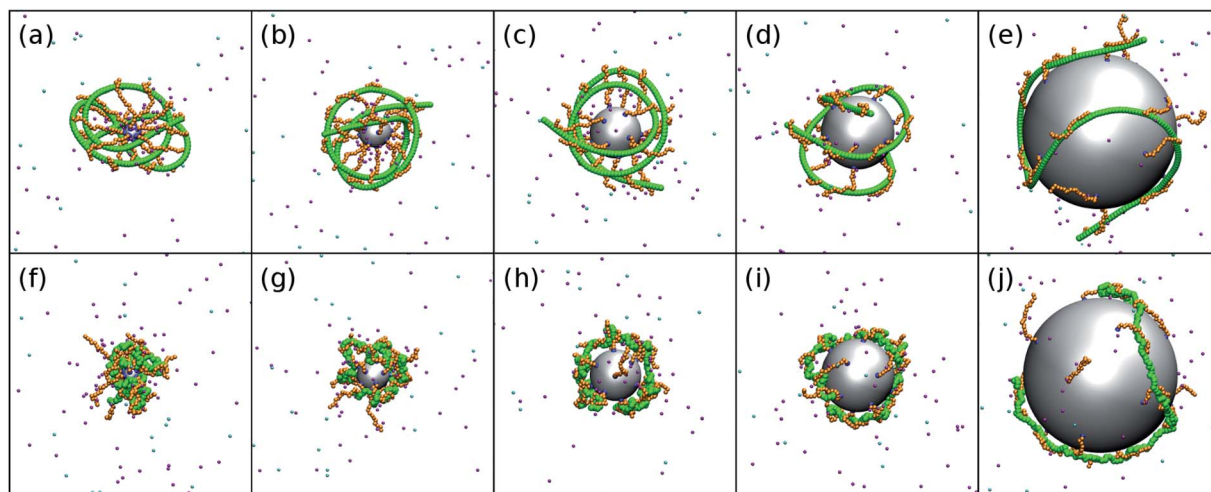


Fig. 5 Typical simulation snapshots of the LPE-SPB complexes at different core radius with $N_g = 15$ and $N_{gm} = 20$. (a)–(e) for the semiflexible LPE correspond to $R = 2\sigma$, 4.5σ , 7σ , 10σ and 21σ , respectively. (f)–(j) for the flexible LPE correspond to the same core radius as (a)–(e).

some grafted chains are not entangled with the LPE due to the increase of the separation between grafting points (Fig. 5e and j), that is, the probability of contact between the LPE and GPE chains is reduced as discussed above. Clearly, the semiflexible LPE adopts a similar conformation as the flexible LPE and clings onto the core surface. Additionally, the local coil-like structures in the conformation of the flexible LPE disappear at $R = 21\sigma$ and the GPEs which entangle with the LPE also adopt an extended conformation. At $R = 2\sigma$, the grafted chains are straightened by the tension from the condensed semiflexible LPE (Fig. 5a). Unlike the semiflexible chain, the flexible LPE forms a compact aggregate (Fig. 5f). At intermediate core radius, the flexible LPE is collapsed on the core surface and adopts a randomly coiled structure at the local scale (Fig. 5g–i), while increased stiffness leads to a well-defined wrapped conformation (Fig. 5b–d).

Fig. 6 shows that there is a larger ordering degree for the semiflexible LPE at intermediate core radius. At $R = 21\sigma$, the ordered wrapping of the LPE around the core is damaged. Nevertheless, the intrinsic stiffness and curvature core radius force the stiffer polyelectrolyte to adopt a solenoid-like

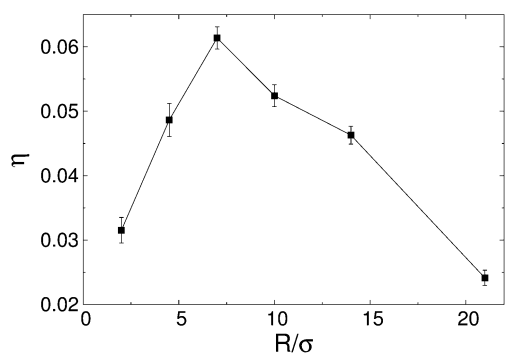


Fig. 6 Dependence of the ordering parameter η of the semiflexible LPE on the core radius R for $N_g = 15$ and $N_{gm} = 20$.

conformation when the core becomes sufficiently large.¹⁴ As observed in Fig. 5e, the LPE is bound to nearby grafting sites, which due to their low density cause a more favorable “S” conformation. At the intermediate radius $R = 7\sigma$, two turns of the LPE binding to the GPE tails and wrapping orderly around the core are found (Fig. 5c). When the core radius is reduced to $R = 2\sigma$, the LPE is highly coiled and located in the plane of its coil conformation. Moreover, the grafted chains are also confined and stretched in the plane. The LPE chain does not exhibit a typical wrapping conformation, and it can form a knot near the core.

To gain a further understanding of the effect of the core radius on the LPE structure, we plot the density distribution function $P(r)$ of the LPE monomers along the radial direction of the core for different core radius in Fig. 7. The peak of $P(r)$ increases with the core radius. At $R = 21\sigma$, the peak becomes very pronounced and its location is closer to the core surface, which indicates that most LPE segments are distributed near

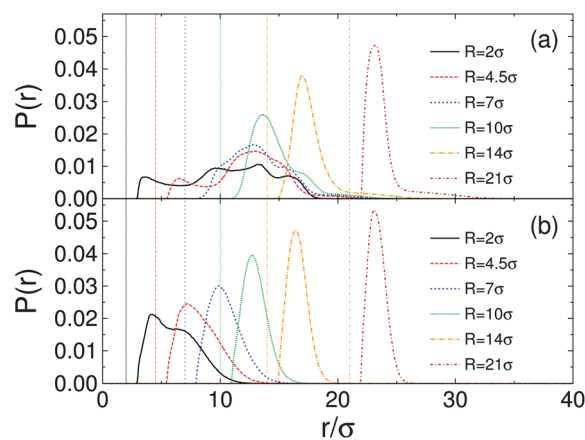


Fig. 7 Distribution function $P(r)$ of monomers for (a) the semiflexible LPE and (b) the flexible LPE along the radial direction of the core at different R for $N_g = 15$ and $N_{gm} = 20$. The vertical lines represent the position of the core surface.

the surface. At $R = 2\sigma$, the slight second peak for the flexible LPE represents a packaging behavior of monomers around the core. When $R \leq 10\sigma$, the distribution profile for the semiflexible LPE contracts as the core radius increases, but its outside (right in this figure) border does not shift significantly. From Fig. 5d to a, we find that the stiffer LPE is strongly “compressed” in a plane if R decreases. However, the largest peripheral size is less influenced in the range of $R \leq 10\sigma$. Instead, the conformation of GPE chains is largely changed (Fig. 4a).

3.3 Effect of the GPE length

The change of the length of grafted chains can influence the conformational behavior of the LPE significantly. As shown in Fig. 8, increasing N_{gm} leads to the detachment of the LPE from the core surface. Here, we limit the total charge of SPB to a fixed value $N_{\text{gm}}N_{\text{g}} = 300$. In particular, the semiflexible LPE chain swells considerably for cases of long GPE chains $N_{\text{gm}} = 30$ and 50 (Fig. 8c and d). When the number of monomers for each GPE is reduced to much smaller values ($N_{\text{gm}} = 1, 5$ in Fig. 8a, b, e and f), the flexible and semiflexible LPEs are adsorbed close to the core surface. In the extreme case $N_{\text{gm}} = 1$, a highly ordered structure of the semiflexible LPE wraps around the core (Fig. 8a), which resembles a single nucleosome.⁴ The tails of the long grafted chains are bent by the tight binding to the semiflexible LPE (Fig. 8d). The deflected part of grafted chains (namely the chain segment adsorbed on the LPE) is still in an extended state, and the non-adsorbed segment is also straightened. Note that two ends of the semiflexible LPE are not bent. In contrast, the end segments of grafted chains which are entangled on the ends of the LPE, adopt the extended conformation of end segments of the LPE. In the case of the flexible LPE, not all grafted chains are in contact with the LPE, because of the tight wrapping of the LPE by GPE chains, which repel each other (Fig. 8g and h). At the same grafting density, such phenomenon is not observed in the case of the stiffer LPE. The

more extended conformation of the semiflexible LPE results in an incomplete complexation with grafted chains (only a fraction of GPE monomers binds to the LPE) and also makes grafted chains more easily approach the LPE. When the length of GPE chains increases and becomes much larger than the size of the core, the brush assumes a star-like shape. Therefore, the increase in the length of GPE chains promotes a change in shape of the nanoparticle from a solid charged sphere *via* a polyelectrolyte brush to a star-like polyelectrolyte. In the presence of brush structure, both the radius of the core and the characteristics of grafted layer will become important in determining the conformational behavior of the LPE.

In Fig. 9a, we give the radius of gyration of the LPE and GPE chains as a function of the GPE length at $N_{\text{gm}}N_{\text{g}} = 300$. Undoubtedly, $\langle R_{\text{gg}} \rangle$ and $\langle R_{\text{lg}} \rangle$ increase with the GPE length. They are larger in the case of the stiffer chain and show a linear dependence on N_{gm} . Additionally, it should be noted that $\langle R_{\text{lg}} \rangle$ of the flexible LPE converges to a constant value for $N_{\text{gm}} > 30$.

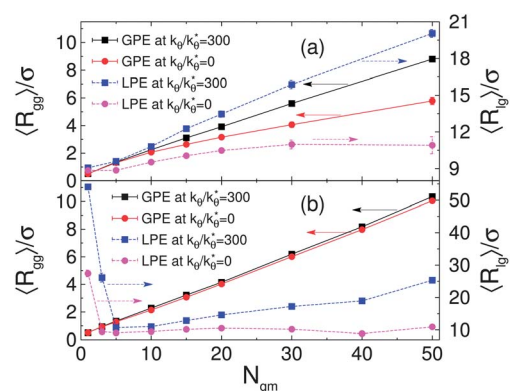


Fig. 9 Average radius of gyration of the LPE ($\langle R_{\text{lg}} \rangle$) and GPE chains ($\langle R_{\text{gg}} \rangle$) as a function of the GPE length for two cases (a) $N_{\text{gm}}N_{\text{g}} = 300$ and (b) $N_{\text{g}} = 40$. The core radius is fixed at $R = 7\sigma$.

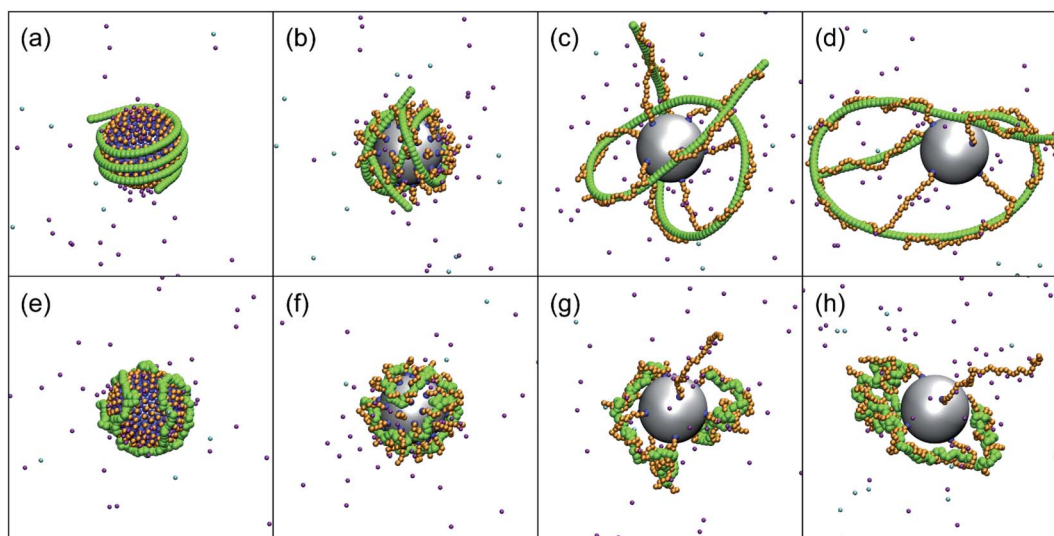


Fig. 8 Snapshots of the LPE-SPB complex at different GPE length and with the fixed total number of GPE monomers $N_{\text{gm}}N_{\text{g}} = 300$ and core radius $R = 7\sigma$. (a)–(d) for the semiflexible LPE correspond to $N_{\text{gm}} = 1, 5, 30$ and 50, respectively. (e)–(h) for the flexible LPE correspond to the same GPE length as (a)–(d).

Further, Fig. 9b shows $\langle R_{gg} \rangle$ and $\langle R_{lg} \rangle$ as a function of the GPE length but at a constant grafting number $N_g = 40$. It is found that $\langle R_{gg} \rangle$ depends linearly on N_{gm} and is insensitive to the LPE stiffness. A maximum value of R_{lg} occurs in the case of bare surface ($N_{gm} = 1$) with low amount of surface charges. This corresponds to an extended chain conformation as shown in Fig. 10a and d. One can observe that the middle segment of the semiflexible LPE is slightly bent (Fig. 10a). In the flexible case, only a segment of the LPE adsorbs to the nanoparticle, because few surface charges are available for binding (Fig. 10d). When increasing the GPE length to $N_{gm} = 5$, the LPE undergoes a collapse transition and most monomers are confined in the vicinity of the core (Fig. 10b and e). Two short tails of the semiflexible LPE, which are not complexed with the grafted chains, are present in straight conformation (Fig. 10b). Further increasing the GPE length leads to the release of bending energy of the semiflexible LPE and a more extended conformation is observed (Fig. 10c). Such behavior is not obvious for the flexible LPE (Fig. 10f and 9b). At $N_{gm} = 50$, the flexible LPE wraps around the core in a random corolla structure. This characteristic conformation differs from the conformation of the flexible LPE at $N_{gm} = 5$ in that the LPE randomly winds around the entire surface (Fig. 10e). It indicates that the chain motion of

the LPE is hindered by long grafted chains. Unlike the flexible LPE, the semiflexible chain adopts a crossing shape and has an average size in its plane comparable to the SPB. Additionally, one can note that the semiflexible LPE does not wrap around the core but rather locates at its side, and the crossing point of the LPE is close to the core (Fig. 10c). It is clear that the number of accessible grafted chains for the LPE is sufficient so that there are many grafted chains which do not complex to the LPE and freely extend in solution.

Fig. 11 shows the ordering parameter of the semiflexible LPE as a function of the GPE length at two different cases of $N_{gm}N_g = 300$ and $N_g = 40$. At $N_{gm}N_g = 300$, increasing N_{gm} results in a decreased ordering degree. As shown in Fig. 8a, when the SPB degenerates to the charged sphere, the semiflexible LPE is in a highly ordered wrapping state. At the fixed grafting number $N_g = 40$, a high ordering density is observed in a range of $N_{gm} = 5$ to 15. For short GPE chains, the incomplete wrapping of the semiflexible LPE leads to low ordering degree. When the GPE becomes longer, the LPE does not exhibit a well-defined wrapping conformation.

3.4 Complexation degree

In the preceding sections we studied the conformational behavior of the complex at different system parameters. In this section, we address the effects of the grafting density, GPE length, core radius and LPE stiffness on the complexation degree of the LPE with the GPEs. To quantitatively study the complexation degree between the LPE and grafted chains, we calculate the ratio $\chi = \langle N_{ads} \rangle / N_{lm}$ where $\langle N_{ads} \rangle$ denotes the average number of GPE monomers which are in contact with the LPE. $\langle N_{ads} \rangle$ can be obtained by counting all monomers of grafted chains within a sphere centered at the center of mass of each LPE monomer and with the cutoff radius $r_c = 1.5\sigma$. Each monomer of a grafted chain is counted only once.

Fig. 12 shows the complexation degree as a function of N_g . For cases of low grafting densities, there are more non-complexed LPE monomers due to less monomers of grafted chains. Therefore, a larger number of grafted chains N_g will promote a rapid complexation. By increasing the grafting density further, a relatively slow increase of χ is observed in the case of the

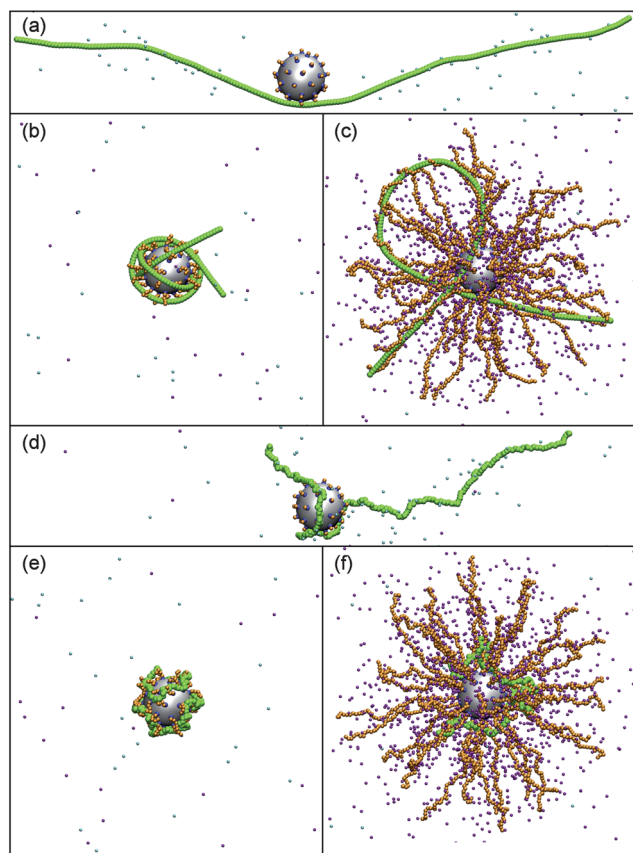


Fig. 10 Simulation snapshots of the complex of the LPE with the SPB for different GPE length: (a) $N_{gm} = 1$, (b) 5, and (c) 50 for the semiflexible LPE; (d) $N_{gm} = 1$, (e) 5, and (f) 50 for the flexible LPE. The grafting number is $N_g = 40$, and the core radius is $R = 7\sigma$.

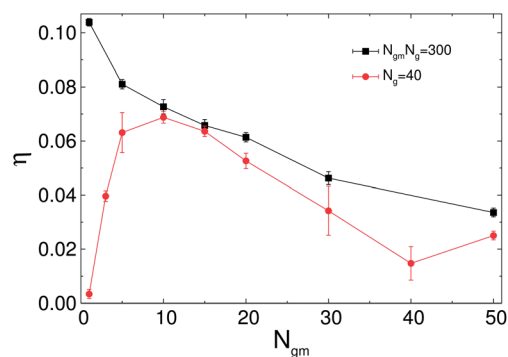


Fig. 11 Effect of the GPE length on the ordering parameter η of the semiflexible LPE wrapping around the core for two different cases: $N_{gm}N_g = 300$ and $N_g = 40$. The core radius is fixed at $R = 7\sigma$.

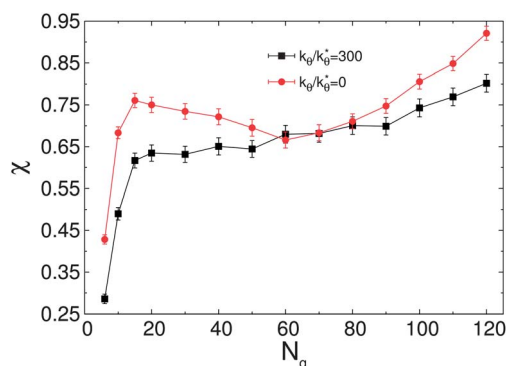


Fig. 12 Complexation degree χ of the LPE with the GPE chains as a function of the grafting number with $N_{\text{gm}} = 20$ and $R = 7\sigma$.

semiflexible LPE. This indicates that a significant amount of LPE monomers are neutralized by monomers of grafted chains. Moreover, counterion condensation in the brush layer becomes also stronger. This suppresses the binding of grafted chains to the LPE. However, for the flexible LPE, the complexation degree decreases at $N_g > 5$ and then increases when $N_g > 60$. At $N_g \approx 15$, the flexible LPE has already reached a high complexation with grafted chains. Instead, further increasing the grafting density leads to a decrease of χ . The complexation degree is enhanced at higher grafting densities. It is believed that the higher density of GPE monomers, which enhances the probability of contacts with LPE monomers, contributes to this increase of χ .

The complexation degree as a function of the GPE length at $N_{\text{gm}}N_g = 300$ is presented in Fig. 13a. In the case of bare core surface, the complexation degree shows a small difference for flexible and semiflexible LPE chains. High surface charge density strongly confines the LPE to the core surface, which corresponds to more contacts with surface particles. For long GPE chains with $N_{\text{gm}} = 50$, the complexation degree for the flexible LPE is almost equal to that for the semiflexible LPE and also becomes larger compared to shorter GPE chains. This indicates that long grafted chains are more supportive of complexation. If longer GPE chains are grafted to the core, the

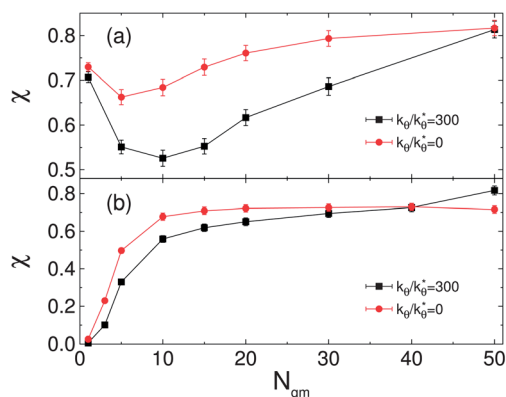


Fig. 13 Dependence of the complexation degree χ on the GPE length for (a) $N_{\text{gm}}N_g = 300$ and (b) $N_g = 40$ with $R = 7\sigma$.

number of grafted chains is decreased (such as $N_{\text{gm}} \geq 100$ and $N_g \leq 3$). The core has almost no effect anymore because the GPE length is much larger than the core size. Additionally, there are only few GPEs grafted on the core surface, and the LPE length is comparable to the GPE length. Therefore, complex formation between the LPE and GPE chains becomes simple for this case, which is similar to the aggregation of two oppositely charged polyelectrolytes.⁵⁹ The semiflexible LPE adopts an entirely extended conformation. It is found that a minimum value appears for relatively short GPE. In cases of shorter GPE, such as $N_{\text{gm}} < 10$ at $k_\theta = 300k_\theta^*$ and $N_{\text{gm}} < 5$ for the flexible LPE, increasing the GPE length weakens the interchain complexation. One can speculate that in this range, many short GPE chains can hardly reach the LPE. Apart from the bare surface and $N_{\text{gm}} = 50$, the LPE rigidity starts to play an important role in controlling the complexation degree. Fig. 13 clearly illustrates that at intermediate GPE length the complexation is much stronger for the flexible LPE.

The dependence of the complexation degree on the GPE length for fixed number of grafted chains $N_g = 40$ is shown in Fig. 13b. At $N_{\text{gm}} = 1$ the complexation degree is nearly zero because of rare surface charges, though a long segment of the flexible LPE is wrapped around the core (Fig. 10d). A remarkable increase of the complexation degree occurs at $N_{\text{gm}} < 10$. For $N_{\text{gm}} > 10$, a plateau value for the flexible LPE is reached (about 0.75). We find that the conformation of the flexible LPE is affected weakly by the GPE length if $N_{\text{gm}} > 20$. It adopts a corolla-like conformation wrapped near the core similar to the case of $N_{\text{gm}} = 50$ (Fig. 10f). The discrepancy is reduced significantly as N_{gm} approaches to $N_{\text{gm}} = 40$. When N_{gm} is larger than 40, the swelling semiflexible LPE has a higher complexation degree with long GPE chains.

The relation between the complexation degree and the core radius is illustrated in Fig. 14. At $R = 2\sigma$, there is a strong complexation of the flexible LPE with GPEs. At $4.5\sigma < R < 10\sigma$, the flexible LPE and most GPE chains twist together and the change of the spacing between grafting sites induced by the core radius does not influence χ . However, in this range of R the complexation degree for the stiffer LPE becomes larger upon increasing the core radius. Decreasing the core radius leads to the increase of charged monomer density within the soft

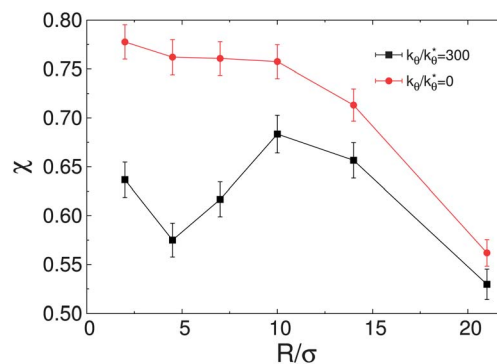


Fig. 14 Complexation degree χ as a function of the core radius at $N_g = 15$ and $N_{\text{gm}} = 20$.

nanoparticle. Meanwhile, the stiffer LPE is also contracted. To balance out the chain bending energy, the electrostatic attractive energy also increases. Interestingly, the complexation degree is reduced. This cannot be explained from a viewpoint of energetics. For the semiflexible LPE, the complexation degree which is calculated in a short range does not represent the magnitude of electrostatic attraction between the LPE and GPE chains due to the long-range behavior of electrostatic force. The decrease of the complexation degree is mainly related to an enhanced release of the LPE from the GPE arms with decreasing the core radius. Considering these factors, the complexation is weakened when the core radius decreases up to $R \approx 4.5\sigma$ in the present set of parameters. However, a further decrease of the core radius, such as $R = 2\sigma$, induces a larger complexation degree. From Fig. 5a, we observe that the conformational energy is minimum, if the complex adopts a planar conformation. Due to the two-dimensional restriction in the configuration, there are more opportunities for forming contacts between the LPE and GPE layer. When the core radius exceeds $R > 10\sigma$, a significant drop of χ is observed irrespective of the chain rigidity. This indicates that the core radius becomes large enough that the LPE bound to neighboring GPEs is out of reach for some grafted chains.

4 Conclusions

By means of extensive molecular dynamics simulations, we have systematically investigated the physisorption and complex formation of a negatively charged long polyelectrolyte with a soft nanoparticle in implicit solvent. The nanoparticle is composed of an impenetrable solid spherical core and a layer of flexible, positively charged polyelectrolytes uniformly grafted to the core. In our coarse-grained model, complex formation of the long polyelectrolyte (LPE) with the grafted polyelectrolytes (GPEs) is governed by electrostatic interaction between all charges (including counterions that ensure neutrality of the entire system), as well as by van der Waals forces. The main goal of this study was to find out how system parameters such as the bending rigidity of the LPE, the density and the lengths of the GPEs, and the core radius influence the formation and shape of LPE–nanoparticle complexes.

The main conclusions are:

- Effect of grafting density. For fixed core radius and GPE length, the LPE–GPE complex is particularly compact, if the number of GPEs is sufficiently large to bind the LPE close to the core surface. On the other hand, if the GPE layer is too dense, electrostatic repulsion of the GPEs that needs to be compensated by the accommodation of counterions effectively pushes the LPE away from the core surface. An optimal grafting density exists for the flexible as well as for the semiflexible LPE. As expected, the semiflexible LPE wraps around the nanoparticle in a more ordered way than the flexible LPE. However, it is quite interesting that the conformation of the semiflexible LPE is highly ordered, if the LPE and the GPEs are most compact (according to their radii of gyration), *i.e.*, there is a correlation between optimal grafting density, maximum compactness of GPEs and LPE, and highest order degree of the LPE.

- Effect of core radius. If the core radius is changed, but all other parameters are kept constant, the most interesting consequence is that the LPE chooses different strategies to optimize the binding to the nanoparticle. It wraps the nanoparticle in layers, if the core radius is small enough such that the grafting density of the GPEs is high and the LPE is much longer than the circumference of the core. Contrary, for sufficiently large core radii, the effective GPE grafting density is dilute and the comparatively short LPE is literally forced to effectively physisorb to the core by forming an “S” shape conformation.

- Effect of grafting density *vs.* number of GPEs. Another interesting case is to keep the total number of GPE monomers constant, but to equally change the GPE grafting density and the GPE length. In the extreme case of a single-monomer GPE, the core surface possesses a uniform pattern, which is attractive for the LPE. A maximum contact number between LPE and GPE monomers can be achieved in a very orderly fashion, although looking differently, for both the flexible and the semiflexible LPE. Only in this case, the LPE–nanoparticle complex resembles a DNA–histone complex. For long but few GPEs, the flexible LPE forms a corona-like shape. Since all LPE charges are saturated by contacts with GPE charges, this is also the minimally compact conformation for the flexible LPE, *i.e.*, increasing the GPE length does not lead to an increase of the radius of gyration of the flexible LPE anymore. This is different for the semiflexible LPE, which is effectively pushed away from the core, if the GPE length is increased (GPE and LPE gyration radii are highly correlated with each other in this case).

- Effect of GPE length. If only the GPE length is changed, the effect is comparable to the above discussed case of changing the grafting density. For sufficiently long GPEs, the nanoparticle looks like a star-like brush. The local GPE density is so high that the GPE “tentacles” strongly repel each other and point away from the core surface, virtually in the direction of the normal surface vector. The repulsion is partly compensated by the binding of the LPE, which penetrates into the brush, and partly by an increased number of counterions that “condensate” in the brush. The semiflexible LPE does not even recognize the spherical shape of the nanoparticle anymore, as the GPEs bend it away from the core. If the GPEs are very short and the density low, the LPE bind only incompletely to the nanoparticle, in which case the complex is weak, *i.e.*, the number of LPE–GPE contacts is small.

These findings are relevant for the design of soft nanoparticles, as we have shown that the strength of the binding between LPEs and GPEs can be controlled by the geometric parameters of the system. A rather weak binding is certainly preferential, if the nanoparticle acts as a transporter of an LPE that has to be released at its destination. Strong binding is desirable, if the nanoparticle is supposed to remove LPEs from an environment. This can be a dedicated “garbage collector” or a nanodevice that functions as a sensor. Our study is a first step to a systematic understanding of the conformational properties of LPE–GPE complexes. Future studies may complement this by thermodynamic analyses of the influence of changes in environmental parameters such as temperature and pressure upon

structural transitions leading to creation or dissolution of such a complex. We hope that the features we predict on the basis of our coarse-grained approach motivate an experimental verification.

Acknowledgements

We are grateful for support by the NSF Grant DMR-1207437.

References

- 1 A. V. Dobrynin and M. Rubinstein, *Prog. Polym. Sci.*, 2005, **30**, 1049–1118.
- 2 R. R. Netz and D. Andelman, *Phys. Rep.*, 2003, **380**, 1–95.
- 3 K. van Holde and J. Zlatanova, *Proc. Natl. Acad. Sci. U. S. A.*, 1996, **93**, 10548–10555.
- 4 K. K. Kunze and R. R. Netz, *Phys. Rev. Lett.*, 2000, **85**, 4389–4392.
- 5 L. Zhang and Y. X. Zhu, *Soft Matter*, 2009, **5**, 4290–4296.
- 6 C. A. Davey, D. F. Sargent, K. Luger, A. W. Maeder and T. J. Richmond, *J. Mol. Biol.*, 2002, **319**, 1097–1113.
- 7 A. U. Bielinska, J. F. Kukowska-Latallo and J. R. Baker, *Biochim. Biophys. Acta, Gene Struct. Expression*, 1997, **1353**, 180–190.
- 8 A. G. Cherstvy and R. G. Winkler, *J. Phys. Chem. B*, 2005, **109**, 2962–2969.
- 9 E. M. Mateescu, C. Jeppesen and P. Pincus, *Europhys. Lett.*, 1999, **46**, 493–498.
- 10 S. Y. Park, R. F. Bruinsma and W. M. Gelbart, *Europhys. Lett.*, 1999, **46**, 454–460.
- 11 P. Chodanowski and S. Stoll, *Macromolecules*, 2001, **34**, 2320–2328.
- 12 P. Chodanowski and S. Stoll, *J. Chem. Phys.*, 2001, **115**, 4951–4960.
- 13 S. Stoll and P. Chodanowski, *Macromolecules*, 2002, **35**, 9556–9562.
- 14 S. Ulrich, A. Laguerre and S. Stoll, *Macromolecules*, 2005, **38**, 8939–8949.
- 15 R. Messina, C. Holm and K. Kremer, *J. Chem. Phys.*, 2002, **117**, 2947–2960.
- 16 A. Akinchina and P. Linse, *Macromolecules*, 2002, **35**, 5183–5193.
- 17 A. Akinchina and P. Linse, *J. Phys. Chem. B*, 2003, **107**, 8011–8021.
- 18 T. D. Yager, C. T. McMurray and K. van Holde, *Biochemistry*, 1989, **28**, 2271–2281.
- 19 A. G. Cherstvy and R. G. Winkler, *Phys. Chem. Chem. Phys.*, 2011, **13**, 11686–11693.
- 20 M. Behnke and B. Tieke, *Langmuir*, 2002, **18**, 3815–3821.
- 21 C. von Ferber and H. Lowen, *J. Chem. Phys.*, 2003, **118**, 10774–10779.
- 22 S. V. Lyulin, A. A. Darinskii and A. V. Lyulin, *Macromolecules*, 2005, **38**, 3990–3998.
- 23 C. Simmons, S. E. Webber and E. B. Zhulina, *Macromolecules*, 2001, **34**, 5053–5066.
- 24 S. Schnabel, T. Vogel, M. Bachmann and W. Janke, *Chem. Phys. Lett.*, 2009, **476**, 201–204.
- 25 S. Schnabel, M. Bachmann and W. Janke, *J. Chem. Phys.*, 2009, **131**, 124904.
- 26 D. T. Seaton, T. Wüst and D. P. Landau, *Phys. Rev. E: Stat., Nonlinear, Soft Matter Phys.*, 2010, **81**, 011802.
- 27 S. Schnabel, D. T. Seaton, D. P. Landau and M. Bachmann, *Phys. Rev. E: Stat., Nonlinear, Soft Matter Phys.*, 2011, **84**, 011127.
- 28 D. T. Seaton, S. Schnabel, D. P. Landau and M. Bachmann, *Phys. Rev. Lett.*, 2013, **110**, 028103.
- 29 C. Junghans, M. Bachmann and W. Janke, *Phys. Rev. Lett.*, 2006, **97**, 218103.
- 30 C. Junghans, M. Bachmann and W. Janke, *J. Chem. Phys.*, 2008, **128**, 085103.
- 31 S. Karalus, W. Janke and M. Bachmann, *Phys. Rev. E: Stat., Nonlinear, Soft Matter Phys.*, 2011, **84**, 031803.
- 32 M. Bachmann and W. Janke, *Phys. Rev. Lett.*, 2005, **95**, 058102.
- 33 M. Bachmann and W. Janke, *Phys. Rev. E: Stat., Nonlinear, Soft Matter Phys.*, 2006, **73**, 041802.
- 34 M. Möddel, M. Bachmann and W. Janke, *J. Phys. Chem. B*, 2009, **113**, 3314–3323.
- 35 T. Vogel and M. Bachmann, *Phys. Rev. Lett.*, 2010, **104**, 198302.
- 36 J. Rühle, M. Ballauff, M. Biesalski, P. Dziezok, F. Grohn, D. Johannsmann, N. Houbenov, N. Hugenberg, R. Konradi, S. Minko, M. Motornov, R. R. Netz, M. Schmidt, C. Seidel, M. Stamm, T. Stephan, D. Usov and H. N. Zhang, *Adv. Polym. Sci.*, 2004, **165**, 79–150.
- 37 R. Toomey and M. Tirrell, *Annu. Rev. Phys. Chem.*, 2008, **59**, 493–517.
- 38 F. Zhou and W. T. S. Huck, *Phys. Chem. Chem. Phys.*, 2006, **8**, 3815–3823.
- 39 Y. Mei, G. Sharma, Y. Lu, M. Ballauff, M. Drechsler, T. Irrgang and R. Kempe, *Langmuir*, 2005, **21**, 12229–12234.
- 40 B. Yameen, M. Ali, R. Neumann, W. Ensinger, W. Knoll and O. Azzaroni, *Nano Lett.*, 2009, **9**, 2788–2793.
- 41 F. Zhou, W. M. Shu, M. E. Welland and W. T. S. Huck, *J. Am. Chem. Soc.*, 2006, **128**, 5326–5327.
- 42 P. Pincus, *Macromolecules*, 1991, **24**, 2912–2919.
- 43 O. V. Borisov, T. M. Birshtein and E. B. Zhulina, *J. Phys. II*, 1991, **1**, 521–526.
- 44 H. Ahrens, S. Forster, C. A. Helm, N. A. Kumar, A. Naji, R. R. Netz and C. Seidel, *J. Phys. Chem. B*, 2004, **108**, 16870–16876.
- 45 E. B. Zhulina, O. V. Borisov and T. M. Birshtein, *J. Phys. II*, 1992, **2**, 63–74.
- 46 R. Israels, F. A. M. Leermakers, G. J. Fleer and E. B. Zhulina, *Macromolecules*, 1994, **27**, 3249–3261.
- 47 A. A. Mercurieva, T. M. Birshtein, E. B. Zhulina, P. Iakovlev, J. van Male and F. A. M. Leermakers, *Macromolecules*, 2002, **35**, 4739–4752.
- 48 L. Samokhina, M. Schrunner and M. Ballauff, *Langmuir*, 2007, **23**, 3615–3619.
- 49 Q. Q. Cao, C. C. Zuo and L. J. Li, *Phys. Chem. Chem. Phys.*, 2011, **13**, 9706–9715.
- 50 R. Ni, D. Cao, W. Wang and A. Jusufi, *Macromolecules*, 2008, **41**, 5477–5484.

- 51 K. Kremer and G. S. Grest, *J. Chem. Phys.*, 1990, **92**, 5057–5086.
- 52 R. W. Hockney and J. W. Eastwood, *Computer Simulation Using Particles*, Adam Hilger, New York, 1988.
- 53 G. S. Grest and K. Kremer, *Phys. Rev. A: At., Mol., Opt. Phys.*, 1986, **33**, 3628–3631.
- 54 L. Verlet, *Phys. Rev.*, 1967, **159**, 98–103.
- 55 M. Allen and D. Tildesley, *Computer simulation of liquids*, Oxford University Press, New York, 1989.
- 56 S. Plimpton, *J. Comput. Phys.*, 1995, **117**, 1–19.
- 57 T. Sakaue, K. Yoshikawa, S. H. Yoshimura and K. Takeyasu, *Phys. Rev. Lett.*, 2001, **87**, 078105.
- 58 Q. Q. Cao, C. C. Zuo, Y. H. Ma, L. J. Li and Z. Zhang, *Soft Matter*, 2011, **7**, 506–514.
- 59 R. G. Winkler, M. O. Steinhauser and P. Reineker, *Phys. Rev. E: Stat., Nonlinear, Soft Matter Phys.*, 2002, **66**, 021802.
- 60 W. Humphrey, A. Dalke and K. Schulten, *J. Mol. Graphics*, 1996, **14**, 33–38.